A Simulation Model of Biofilms with Autonomous Cells, 2 - Explicit Representation of the Extracellular Polymeric Substance[a]

Yu-Guo Tao,* Gary W. Slater*

Biofilms are complex colonies of bacteria that grow in contact with a wall, often in the presence of a water flow. In the current work, biofilm colony growth is investigated using a two-dimensional lattice Monte–Carlo algorithm based on the bond-fluctuation algorithm (BFA). One of the distinguishing characteristics of biofilms, the synthesis and physical properties of the extracellular polymeric substance (EPS) in which the cells are embedded, is explicitly taken into account. Cells are modeled as autonomous closed loops with well-defined mechanical and biological properties, while the EPS is modeled as flexible polymeric chain synthesized by the cells during their growth. By tuning the structural, energy, biological, and morphologic parameters of the model, the cell shapes as well as the growth and maturation of various types of biofilm colonies (including colonies with multiple species) can be controlled.

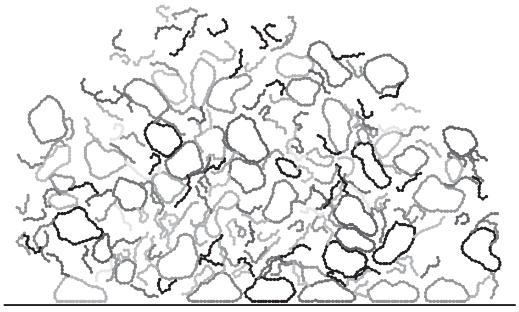

Introduction

A biofilm is an entity composed of a huge number ($\sim 10^9$–10^{12}) of microorganisms that grow on surfaces and in the presence of an aqueous environment. They secrete a polymeric substance which serves as a binding agent as well as a shield against external attacks. These microorganisms may form multi-species communities with complex relationships. Motility, cell–cell signaling, and mutations are among the biofilm characteristics that play an important role in their ability to resist antimicrobial treatments.[1,2]

Y.-G. Tao, G. W. Slater
Department of Physics, University of Ottawa, 150 Louis-Pasteur, Ottawa, Ontario, Canada K1N 6N5
E-mail: ytao@uOttawa.ca, gary.slater@uOttawa.ca

[a] Part 1: cf. Ref.[34].

Modeling a microbial system is a tremendous task because of the number of structural, chemical, and kinetic parameters that need to be taken into account. Several models[3] have been proposed for studying the growth and morphology of biofilms. Based on different spatial and biomass representations, these models can be categorized into: the Cellular Automata (CA) methods;[4–17] the individual-based models (IbM);[18–25] and the continuum models.[26–33] These models have allowed the study of several aspects of microbial ecology such as pattern formations, group competition and cooperation within biofilms, and multi-species biofilm structures. However, sophisticated they may be, these models (like all models) suffer from various weaknesses. For instance, space and biomass are discrete variables in the CA models; the IbM do not give a physical or mechanical representation of bacterial cells which generally means that some ad hoc rules must be used; the continuum models are suitable for modeling systems with large-scale heterogeneities, but cannot be used to study local properties or the impact of

DOI: 10.1002/mats.201100030

various initial states. With the continuous improvements in computational capabilities, the implementation of models with more detailed information has become possible. Our model,[34] which we believe is among the most detailed models for biofilm to date, is coarse-grained to the cellular level — the cells are autonomous agents with mechanical, biological, and thermodynamic properties.

The extracellular polymeric substance (EPS), which is secreted by the cells,[35,36] forms an embedding matrix that serves both as a binding agent for the colony (thus directly affecting its morphology) and a shield against external attacks. In nature, EPS molecules are generally complex mixtures of proteins, carbohydrates, lipids, DNA, nucleic acids, amphiphilic polymers, etc. They are believed to serve many functions including: (i) the promotion of the initial attachment of the cells to the surface on which the biofilm is growing; (ii) the exchange of genetic material between the cells; (iii) the formation and the maintenance of the biofilm structure; (iv) the resistance of biofilm to the many environmental stresses it may encounter; and (v) the enhancement of the interactions between the bacteria and their bio-physicochemical environment. In addition, the EPS matrix also enables the bacteria to capture (avoid) nutrients (toxic molecules) in many cases. In the present article, we introduce a few modifications to the model as well as a method to explicitly include simplified EPS molecules, and we test these new model elements for cells in a stagnant aqueous environment.

This paper is structured as follows. A Cell-Based Lattice Monte–Carlo Model For Biofilm Simulation Section first summarizes our lattice Monte–Carlo (LMC) model (described in detail in Tatek and Slater[34]). The dynamics of the most important addition of the model, the EPSs, is included. We also review the fact that in this model, the growth of biofilm colonies is examined by considering many factors, such as cell growth, EPS growth, cell division, cell death, cell maintenance, EPS detachment, etc. Shape and Size of Cells Section gives details of an extensive analysis of individual features and parameters of the model. In Interactions with EPS Chains Section we examine how microbial cells (with EPS chains attached to their membranes) interact with each other and with their environment at a microscopic scale. Examples of the growth of a biofilm/EPS colony are given in Examples of EPS–Cell Biofilms Section, and in Conclusion Section we conclude with a summary.

A Cell-Based Lattice Monte–Carlo Model for Biofilm Simulation

The Basic Elements of Our Bond Fluctuation Model

We previously introduced a two-dimensional (2D) LMC algorithm for biofilm simulation,[34] but this model lacked a representation for the polymeric EPS chains. The model coarse-grains the system at the cellular level and allows us to easily incorporate cell interactions and important cell activities like growth, division, maintenance, motility, and death. The bond-fluctuation algorithm (BFA),[37] borrowed from computational polymer science, simplifies the simulation problem to a list of rules that govern how "particles" move on the lattice. By linking these particles in different ways, system components like the cells, the surrounding walls, and the nutrients can be explicitly defined. Specific potentials can be used to define interactions between these elements, and external fields can be used to influence their motion. The model can be completely defined with these features, subject to boundary and initial conditions (which may include the continuous injection of nutrients). The 2D BFA implemented in this model uses a square lattice with a plaquette being the smallest object (four lattice sites forming a square plaquette); these plaquettes are subjected to volume exclusion hard core interactions and can be used as *monomers* in order to build the cell membrane, the EPS chains, wall surfaces, or other system components. Monomers are only allowed jumps by one lattice site along either of the four Cartesian directions ($\pm\hat{x}$ or $\pm\hat{y}$). A BFA jump is accepted provided it obeys local rules (such as volume exclusion), and satisfies Metropolis energy tests.[38]

In our model, a cell is defined by a membrane, which is a collection of BFA monomers linked together by bonds to form a closed perimeter. The cell membrane is thus taken to be a ring polymer made up of N_c monomers connected by N_c BFA links. Henceforth, the subscript c will be used to refer to the cell membrane. N_c is allowed to vary but is restricted to be between N_c^0 and $N_c^{max} = 2N_c^0$, where N_c^0 is the minimum cell size. In the framework of the 2D BFA, the bond length between connected monomers is restricted to the range $2 \leq l \leq \sqrt{13}$ (this ensures that chains do not cross). For a free BFA linear chain (no bending potential), the average bond length is approximately 2.93 lattice spacings, while it increases slightly to 3.00 ± 0.06 for the membrane ring polymer when we choose $\kappa_c = 3$ and $\Delta p_c = 0.005$ (the preferred simulation conditions, as we will see later).

The cell being a closed entity, we impose an osmotic pressure difference $\Delta p_c = p_{int} - p_{ext}$ across its membrane. Furthermore, the stiffness of the cell membrane can be modeled using a bending potential related to the angle θ formed between two consecutive bonds (see in Figure 1). In our previous study, we used the form:

$$U_c(\theta) = \kappa_c \times (1 + \cos\theta)^2, \quad (1)$$

where κ_c is the membrane bending rigidity parameter and $\theta \in [0, 2\pi]$. In this paper, we use the alternative form:

$$U_c(\vartheta) = \kappa_c \times (\vartheta - \vartheta_0)^2, \quad (2)$$

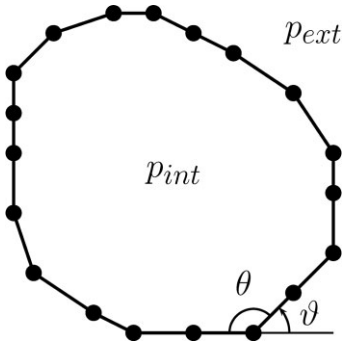

Figure 1. In our current model, a cell is represented by a closed polymer ring. The osmotic pressure difference across the membrane is given by $\Delta p_c = p_{int} - p_{ext}$. There are two ways to define the bending angle between two consecutive bonds: $\theta \in [0, 2\pi]$ and $\vartheta \in [-\pi, \pi]$, as shown.

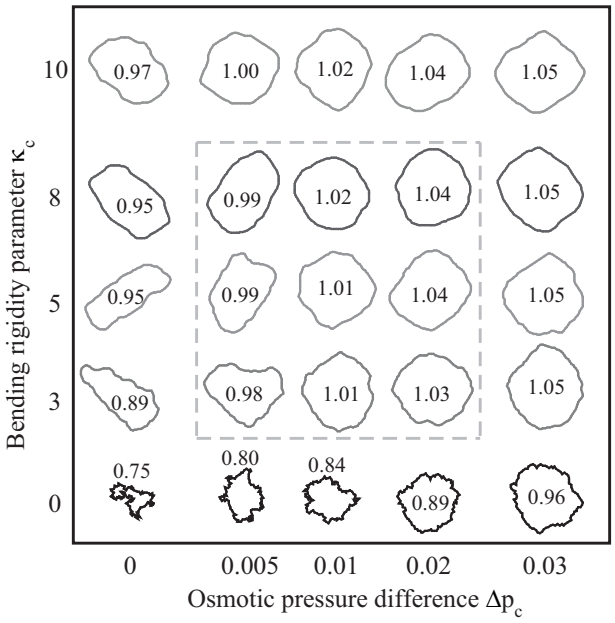

Figure 2. Typical cell shapes in the $\kappa_c - \Delta p_c$ phase space. All cells have $N_c = 100$ monomers. For each combination of parameter, the Flory exponent ν is also given inside (or above) the cell shape.

where $\vartheta = \pi - \theta$ (as shown in Figure 1) and $\vartheta \in [-\pi, \pi]$. Note that the equilibrium bending angle ϑ_0 has a value of $2\pi/N_c$ for a 2D circular-shape cell. It is possible to build different cell shapes if the angle ϑ_0 is not the same for all pairs of bonds along the cell membrane. A complete list of ϑ_0 defines the cell shape; for example, we will show later that this approach allows us to simulate cigar-shaped cells. It is of course also possible to use κ_c to affect the equilibrium cell shape.

The presence of both a pressure gradient Δp_c and a membrane stiffness κ_c ensures that cells automatically adjust to local mechanical stresses. This is important, for example, when cells grow and divide inside a colony. However, these model parameters must be chosen properly in order to obtain cells with realistic shapes and properties. As shown in Figure 2, the shape of a nominally round cell can be quite different when we change these two parameters. In this particular case, the cell should be round, its perimeter should be smooth, and its surface area should increase like N_c^2. The scaling of the surface area $\langle A \rangle$ with the perimeter can be described by the expression $\langle A \rangle \sim N_c^{2\nu}$, where ν is Flory's exponent. The Flory exponent is given in Figure 2 for every cell shape. As mentioned before, this exponent should be around unity for a smooth inflated 2D shape. It is well-known that $\nu = 3/4$ for a closed ring without a pressure difference. Values larger than unity correspond to cases where the parameters are so large that the mean bond length starts increasing, a situation which must be avoided in our model. In the current study, we thus focus our investigation on the parameter regime shown in the dashed frame in Figure 2. As we shall see later, EPS chains attached to the cell actually lead to cell swelling; for this reason, parameters in the bottom-left corner of this marked area (in the vicinity of $\kappa_c = 3$ and $\Delta p_c = 0.005$) will be used in this paper.

One must also choose the structural parameters κ_c and Δp_c to optimize the dynamical features of the cell. Because the BFA is based on a lattice and is characterized by a finite set of bond lengths, certain combinations of parameters actually lead to situations where almost all Monte–Carlo jumps are rejected and where the cells can barely diffuse in space. As can be seen in Figure 3(a), the Monte–Carlo jump rejection rate reaches about $\alpha \approx 90\%$ when κ_c exceeds $\simeq 8$. Obviously, this greatly decreases the efficiency of the simulation. It is also clear from these results that the membrane stiffness has a much larger impact than the pressure gradient. Moreover, the translational diffusion coefficient of the center-of-mass of the cell, D_{CM}, decreases by a factor of $\simeq 4-5$ when the stiffness parameter increases from 0 to 8 (see Figure 3b). When the diffusion coefficient is divided by $1-\alpha$ in order to take into account the increased rejection rate (see Figure 3c), we see that the data nearly collapse on a universal curve that is essentially flat when the cell bending rigidity κ_c does not exceed ~ 7. In the low-κ_c regime, jump rejection seems the only factor that reduces the diffusion of the cell. When $\kappa_c \gtrsim 7$, an almost linear decrease of the ratio $D_{CM}/(1-\alpha)$ indicates that other mechanisms, most likely artifacts due to the simulation algorithm itself, affect the cell dynamics. In conclusion, in order to obtain realistic dynamics and efficient simulations, we will stay in the $\kappa_c < 6$ regime.

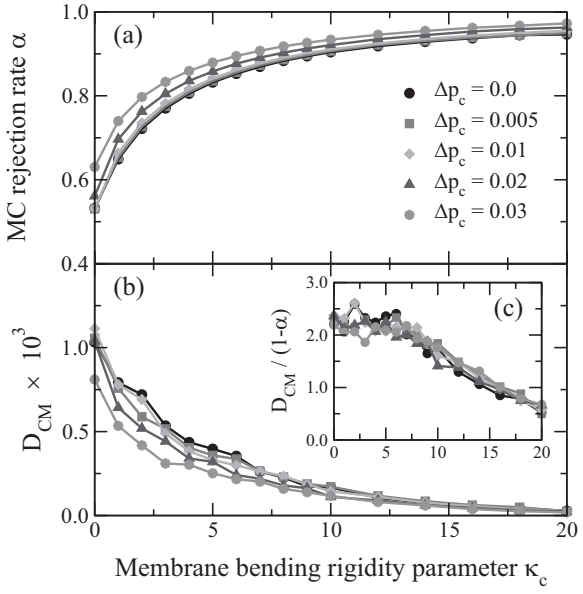

Figure 3. (a) The Monte–Carlo jump rejection rate α and (b) the translational diffusion coefficient D_{CM} of the cell center-of-mass as a function of the membrane bending rigidity parameter κ_c. Values of the osmotic pressure difference ranging from $\Delta p_c = 0$ to 0.03 are shown. The inset panel (c) shows the ratio between the diffusion coefficient D_{CM} and the Monte–Carlo jump acceptance rate $1-\alpha$. A cell of size $N_c = 100$ was used for all simulations.

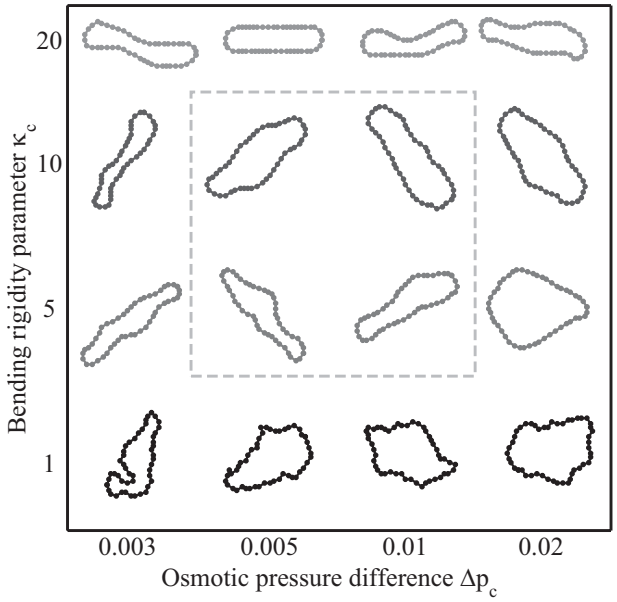

Figure 4. Examples of typical cigar-shape cells with $N_c = 48$ monomers for various bending rigidity parameters κ_c and osmotic pressure differences Δp_c.

In Figure 4 we illustrate 16 different cigar-shaped cells in the $\kappa_c - \Delta p_c$ phase space. Each cell consists of 48 linked monomers and the equilibrium bending angles ϑ_0 are 0 or $\pi/6$ for the flat sides and the spherical end-caps, respectively. Note that the end-cap ϑ_0 depends on the cell size N_c: in order to design a prefect cigar-shape cell with different aspect ratios, the end-cap equilibrium bending angle ϑ_0 needs to be varied. As we can see, the cells have sharp kinks when κ_c is low. On the other hand, the cells are deflated when Δp_c is small. The cell shapes and dynamics are acceptable in the parameter range $\kappa_c \in [5, 10]$ and $\Delta p_c \in [0.005, 0.01]$ in this example (the area in the dashed frame in Figure 4).

In nature, a biofilm colony is formed when a bacteria finds a surface and sticks to it. In our model, the flat surfaces are modeled as a series of adjacent and immobile monomers. Although these wall monomers are immobile, the BFA rules apply when cell (or EPS) monomers touch them.

The last elements of the model are the *substrate* particles (such as food, waste, or toxic molecules). These elements are all represented by a single monomer that diffuses freely in the biofilm colony. Cells absorb nutrient substrate particles in order to grow, maintain their metabolism, etc. To simulate the nutrient intake, an intake probability Γ_{cs} is applied to the substrate particles when they collide with the cell membrane. The particles which have been "eaten" are thus taken out from the simulation box, while a particle counter N_{cs} representing the stored energy or nutrient level of the corresponding cell is incremented by one. In order to model cell self-regulation, the intake probability is itself proportional to the current value of N_{cs} via the relation:

$$\Gamma_{cs} = \Gamma_{cs}^0 \times \left(1 - \frac{N_{cs}}{N_{cs}^{max}}\right), \tag{3}$$

where $\Gamma_{cs}^0 > 0$ is the maximum intake probability, and the maximum allowed level of nutrients inside a cell, N_{cs}^{max}, can be chosen to be arbitrarily large (for simplicity, we often use $N_{cs}^{max} = N_c^0$).

In the absence of potential gradients (e.g., those due to flow or gravity), maintaining the nutrient particle concentration ρ constant far from the colony is a natural choice. Since colony growth takes place on a wall surface (the plane $y = 0$), the simulations are performed between parallel walls $y = 0$ and L. Periodic boundary conditions are imposed on substrate particles, all the while ensuring the simulation box size and the spacing L are much larger than the colony size. As usual in LMC studies, time is measured in Monte–Carlo steps (MCS). One MCS corresponds to one attempted move per mobile particle (membrane, EPS, or substrate) in the system.

Adding EPS Chains

The presence of EPS is a key characteristic of microbial colonies. In the current model, EPS polymers are simply linear chains of BFA monomers. Cells that belong to a colony can start producing polymeric EPS chains regardless of their growth state; these chains grow from randomly selected sites on the membrane. The growth of an EPS chain (attached to the cell membrane) is simulated by adding a monomer at the end or along the backbone of an existing chain. An EPS chain can grow until its length N_e reaches the maximum value N_e^{max}, with the growth probability per unit time governed by:

$$\Gamma_e = \Gamma_e^0 \times \frac{N_e^{max} - N_e}{N_e^{max}} \times \frac{N_{cs}}{N_{cs}^{max}}, \quad (4)$$

where Γ_e^0 is the maximum EPS growth probability. When a monomer is added to a chain ($N_e \rightarrow N_e + 1$), the cell reserves decrease by one unit: $N_{cs} \rightarrow N_{cs} - 1$. Note that a long EPS chain grows more slowly.

A cell can grow n_e EPS chains of size N_e simultaneously (with $0 \leq N_e \leq N_e^{max}$). The attached EPS chains can be distributed randomly or periodically along the membrane (for simplicity, we chose the latter in this study). To model the EPS chains rigidity, we use $\vartheta_0 = 0$ and a bending parameter κ_e in Equation (2).

The EPS chains can detached from the cell in order to form the EPS medium in which the cells are embedded. They do so with a certain rate $\Gamma_{clip} \times N_e / N_e^{max}$, where $\Gamma_{clip} \in [0, 1]$ is a constant; note that longer chains are more likely to be clipped. They also detach when the cell divide in order to minimize the steric constraints.

The use of single-site substrate particles allows the latter to cross the EPS chains (four site BFA monomers would not be able to do this); without this feature, substrate particles would not be able to reach the inside of a colony because of the strong effect of excluded volume interactions in two-dimensions. However, these particles cannot penetrate the cell membrane (they either bounce or are *eaten*).

Cell Growth and Division

These natural phenomena are related to some important aspects of the cell's state: its age t, size N_c, and internal nutrient content N_{cs}. Cell growth is simulated by adding a monomer to the membrane at a random position ($N_c \rightarrow N_c + 1$) without violating the BFA rules. The new monomer is taken from the cell internal resources ($N_{cs} \rightarrow N_{cs} - 1$). The probability of cell growth per unit time, Γ_c, increases linearly with N_{cs} but decreases to 0 when the cell reaches its maximum size:

$$\Gamma_c = \Gamma_c^0 \times \frac{2N_c^0 - N_c}{N_c^0} \times \frac{N_{cs}}{N_{cs}^{max}}, \quad (5)$$

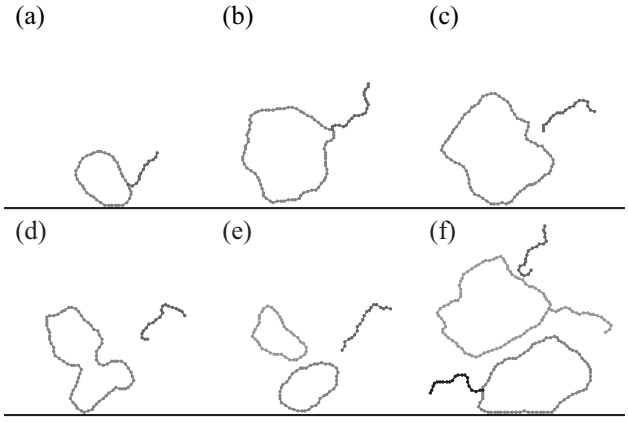

Figure 5. Schematic diagram showing various stages of the biofilm formation: (a) the initial cell finds a wall, attaches to it and grows an EPS molecule. (b) The cell eats nutrient particles diffusing in the environment and, as a result, doubles in size. (c) When the full-size cell reaches its maturity age, cell division can start. In the first stage, the EPS molecules still attached to the cell are clipped. (d) During the second step of the cell division process, two pairs of monomers move towards each other via biased Brownian motion. (e) The bonds linking the membrane monomers are rearranged and two new daughter cells are born. (f) The new-born daughter cells grow up and new linear EPS chains are synthesized. These six stages repeat themselves for each cell; the resulting biofilm thus consists of both cells and free EPS chains.

where Γ_c^0 is the maximum growth probability. In Figure 5, the snapshots illustrate different early stages of a typical biofilm formation. The cell in (Figure 5a) has attached to the wall and a short EPS molecule has started growing. After the cell has doubled in size (Figure 5b) its EPS molecule detaches (Figure 5c) and the cell divides into two (Figure 5d and e). The two new cells double in size and grow EPS molecules (using nutrients in the process), and the process continues (Figure 5f).

Cell maturity, a necessary criterion for cell division, is defined by attainment of the maximum membrane size N_c^{max} ($N_c^{max} = 2N_c^0$) and an age t_{mature}. The probability of cell division per unit time, Γ_{div}, becomes nonzero upon maturity. The dynamics of cell division and membrane rearrangement, as shown in Figure 5(d and e), are described in detail in our previous study.[34] The end result is two daughter cells, shown in Figure 5(e), with N_c^0 membrane monomers each, generally with different surface areas. The amount of internal nutrients N_{cs} initially present in the mother cell is divided equally among the two daughter cells. The volume expansion of the colony is caused by the internal pressure generated by the subsequent growth and relaxation of the newly formed cells and EPS molecules. In other words, our colonies are able to self-adjust to any internal changes.

Local Interactions

Only short-range attractive interactions between the BFA monomers (belonging to the wall surface (w), the cell membrane (c), and the EPS chain (e)) will be considered. Since the minimum allowed distance between two monomers is $\Delta r = 2$ lattice sites in the model, the potential energy between any two monomers can be written as:

$$U_{ij}(\Delta r) = \varepsilon_{ij} \times \delta_{\Delta r,2}, \tag{6}$$

where i and j are the indices indicating the nature of the two monomers involved and δ is the Kronecker Delta. This defines a maximum of five different interaction parameters ε_{ij} (ε_{ww} being irrelevant). In practice, several of these parameters can either take the same (negative) value or be chosen equal to 0.

Shape and Size of Cells

In this section, we investigate the shape properties of a round cell that is decorated by n_e EPS chains of length N_e. In essence, this is similar to having a flexible vesicle coated with a polymer brush. As we shall see, an EPS brush can make the cell swell for entropic reasons.

For this problem, the main parameters are: the cell membrane size N_c, the EPS chain length N_e, the number n_e of EPS chains attached to the cell, the membrane bending rigidity parameter κ_c, the EPS bending rigidity parameter κ_e, and finally the osmotic pressure difference Δp_c. Our investigation will focus on measuring three fundamental geometric quantities: the cell surface area $A = (1/2)\left|\sum_{i=1}^{N_c-1} \mathbf{r}_i \times \mathbf{r}_{i+1}\right|$ (where $\mathbf{r}_i$ is the position of the ith monomer of the cell membrane), and the reduced mean square end-to-end distance $(\langle h^2\rangle/N_e^2)$ and radius of gyration R_g of the flexible EPS chains.

Cells Without EPS Chain

As mentioned previously, the average surface area inside a 2D closed self-avoiding random walk follows the standard scaling law $\langle A\rangle \sim N_c^{2\nu}$, where $\nu = 3/4$ is the Flory exponent. For a well-behaved round cell, one would require that $\nu = 1$ instead. It is the role of the pressure difference and the membrane bending rigidity to increase the Flory exponent in our model. The Flory exponent was given in Figure 2 of A Cell-Based Lattice Monte–Carlo Model for Biofilm Simulation Section for 25 different combinations of Δp_c and κ_c. In this section, we present the raw data that lead to these values.

In Figure 6(a), we examine zero-pressure (i.e., $\Delta p_c = 0$) cells with membrane bending rigidities κ_c ranging from 0 to 5; as we can see, the slope increases from $2\nu = 3/2$ to $2\nu = 2$

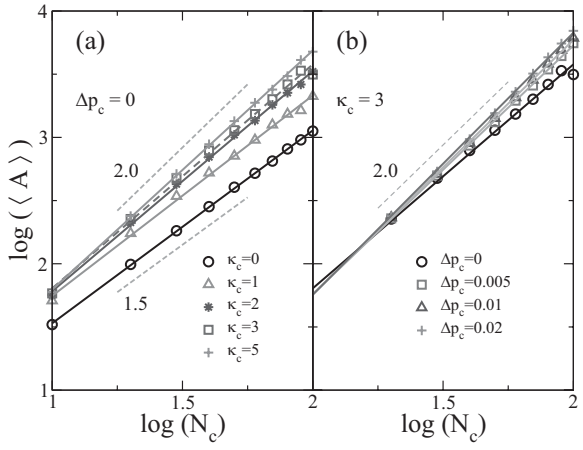

Figure 6. Log–log plot of the mean surface area $\langle A\rangle$ as a function of the cell membrane size N_c. In panel (a), $\Delta p_c = 0$ while the membrane bending rigidity parameter κ_c is varied from 0 to 5. In panel (b), $\kappa_c = 3$, while the pressure difference Δp_c is varied from 0 to 0.02.

as the membrane becomes more rigid. Moreover, the cell clearly swells when κ_c increases. This swelling is due to both a smoothing of the membrane roughness and an increase of the mean BFA bond length. When κ_c exceeds about 5 (see Figure 2), the cell walls actually align along the 45° directions of the lattice in order to maximize the number of bonds with the maximum bond length $\sqrt{13}$. This algorithmic artifact leads to unphysical cell shapes and it should be avoided.

The effect of the osmotic pressure is examined in Figure 6(b) for the case $\kappa_c = 3$ (which represents a good choice based on the results discussed above). The four effective Flory exponents are, from bottom to top, $\nu = 0.89$, 0.98, 1.01, and 1.04. We observe a small amount of chain swelling as Δp_c increases; this is accompanied by larger than unity Flory exponent and some bond alignment along the diagonal directions. Based on these results, we determine that the combination $\kappa_c = 3$ and $\Delta p_c = 0.005$ provides cells with realistic structural properties.

It is also interesting to look at the probability distribution function for the cell surface are A. In the absence of an EPS brush attached to the membrane, the distribution function is not quite Gaussian (see Figure 7, curve **a**). As we shall see later, the presence of a brush makes narrows the distribution function, makes it more Gaussian, and reduces the overall fluctuations of the membrane.

Cells with EPS: Flexible *Versus* Stiff EPS Chains

In the next two sections, we will examine the impact of the EPS stiffness parameter κ_e, the EPS density σ_e (defined as $\sigma_e = n_e/N_c$, where n_e is the number of EPS chains attached to the membrane and N_c is the maximum number of chains

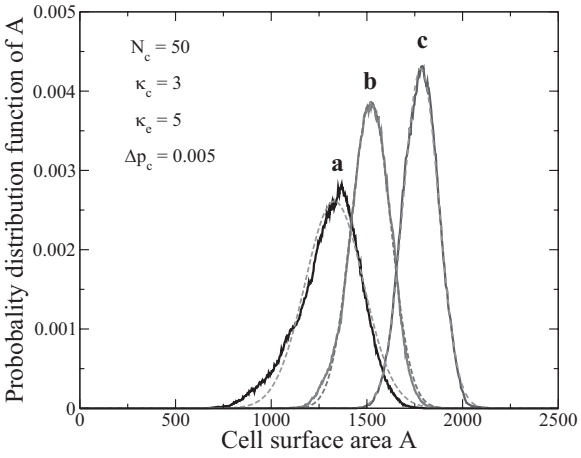

Figure 7. The probability distribution function of the cell surface area A. Solid curves are simulation results; Gaussian fits are shown with dashed lines. In example **a**, there is no EPS chains, while in examples **b** and **c**, we examine cells with EPS chains attached to their membranes: (b) $n_e = 10$ chains with $N_e = 30$ monomers each; (c) $n_e = 25$ chains with $N_e = 10$ monomers each.

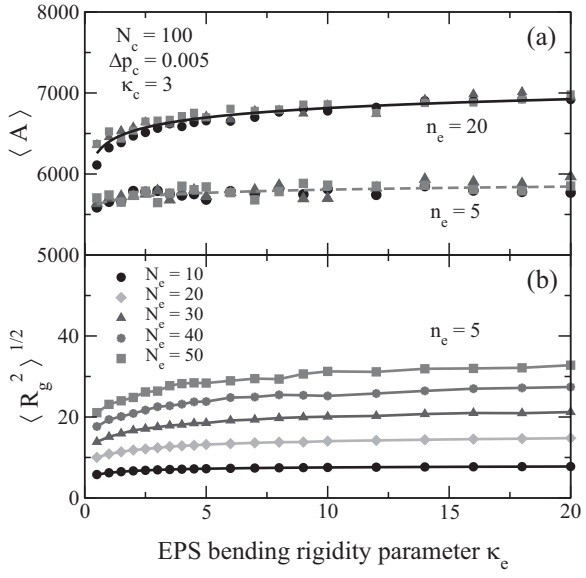

Figure 8. (a) The mean surface area $\langle A \rangle$ and (b) the root mean square radius of gyration of EPS chains, $\langle R_g^2 \rangle^{1/2}$, *versus* the EPS bending rigidity parameter κ_e for five different chain lengths N_e. Two EPS densities, $\sigma_e = 5/100 = 0.05$ and $\sigma_e = 20/100 = 0.2$, are examined in (a), while $\sigma_e = 0.05$ in (b).

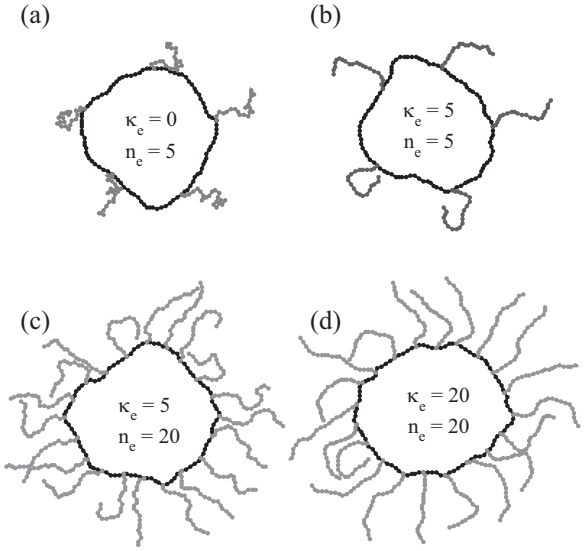

Figure 9. Four typical cell shapes (of size $N_c = 100$) with n_e EPS chains (of size $N_e = 20$) attached. In all simulation, $\kappa_c = 3$ and $\Delta p_c = 0.005$ are applied.

that can be attached to a membrane composed of N_c monomers; therefore, $0 \leq \sigma_e \leq 1$), and the EPS chain length N_e on the structural properties of the cell to which these molecules are attached.

Compared to the membrane bending rigidity parameter κ_c, the related EPS parameter κ_e has little influence on the cell structure even though the persistence length of our EPS chains increases from about one bond when $\kappa_e = 0$ to 14 bonds when $\kappa_e = 20$ (results not shown; note that the average bond length is essentially constant over this range). For instance, at the very low EPS density of $\sigma_e = 0.05$ (lower curve in Figure 8a), the mean cell surface area is essentially constant when κ_e increases from 0.5 to 20, regardless of the length of the EPS chains since the latter interact very little. The surface area $\langle A \rangle$ increases by about 5% over this range of κ_e when the chain density is $\sigma_e = 0.2$ (upper curve in Figure 8a); at this density, the chains have steric interactions with each other, and the resulting entropic repulsion leads to an outward swelling force that increases the mean cell surface area. This effect can be seen in Figure 9 where four different examples are shown. We note that this swelling effect saturates when the chain are very rigid (roughly $\kappa_e > 5$).

It is also interesting to examine the evolution of the root mean square radius of gyration $\langle R_g^2 \rangle^{1/2}$ of the membrane-bound EPS chains when their stiffness parameter κ_e increases (Figure 8b). Not surprisingly, their radius of gyration increase until we reach a plateau (in essence, the plateau is reached when the persistence length of the chain becomes comparable to its contour length). Again, there is very little increase when $\kappa_e > 5$ for these chains. The radius of gyration is found to increase like $R_g \sim N_e^{3/4}$ (typical of a self-avoiding walk) when κ_e is small, but like $R_g \sim N_e^1$ (as expected for a rod-like object) when κ_e is large (data not shown).

Given these results, we will choose $\kappa_e = 5$ in the following since it is roughly the smallest value for which we observe the plateau in Figure 8(a); smaller values would not provide good mechanical properties for the colony, while larger

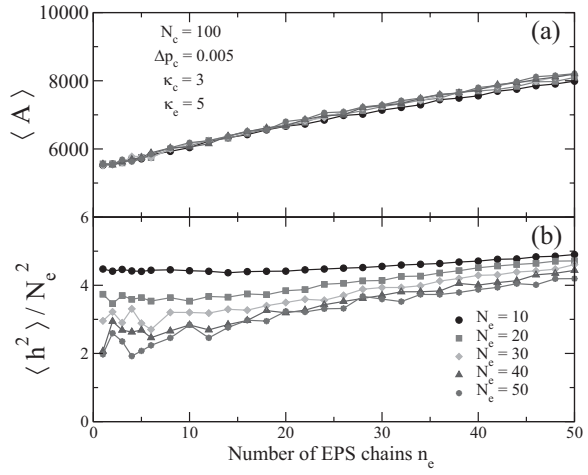

Figure 10. The mean surface area $\langle A \rangle$ and the reduced mean square end-to-end distance $\langle h^2 \rangle / N_e^2$ as a function of the number n_e of EPS chains attached to the membrane.

values would generate very stiff EPS molecules that would have strong nematic interactions.

Cells with EPS: The Density of EPS Chains (σ_e)

In order to accommodate more EPS chains, our BFA cell must increase its surface area as shown in Figure 10(a). Although we observe a small plateau for low chain density (roughly $n_e < 5$ or $\sigma_e < 0.05$ here), the mean surface area increases almost linearly with the number of chains beyond that point for all chain sizes N_e. Interestingly, the EPS reduced mean square end-to-end distance $\langle h^2 \rangle / N_e^2$ (Figure 10b) increases towards a universal value as the number of chains, n_e, increases; this is what is expected in the limit where the chains assume rigid-rod conformations (with $h \sim N_e$) and form a dense brush (see also Figure 9). In fact, we note that this ratio is essentially constant until the density of chains is such that they start having steric repulsive interactions. This happens for lower chain densities when the chain is longer, as expected. We also observe a shallow minimum for intermediate EPS densities (see the $N_e = 10$ and 20 curves); in this regime, cell swelling is accompanied by a small amount of chain collapse due to reduced steric interactions.[39–41]

Since the cell surface area and the EPS chains end-to-end distance remain approximately constant for chain densities $\sigma_e \lesssim 0.05$, we will restrict our simulations to this range. Moreover, the Flory exponent stays near the ideal value of $\nu = 1$ under such conditions (data not shown).

Finally, we note that in the presence of EPS chains, the standard deviation of the average cell surface area is substantially reduced. Figure 7b and c shows two examples demonstrating this effect. Furthermore, the presence of the EPS brush makes the probability distribution function more Gaussian-like.

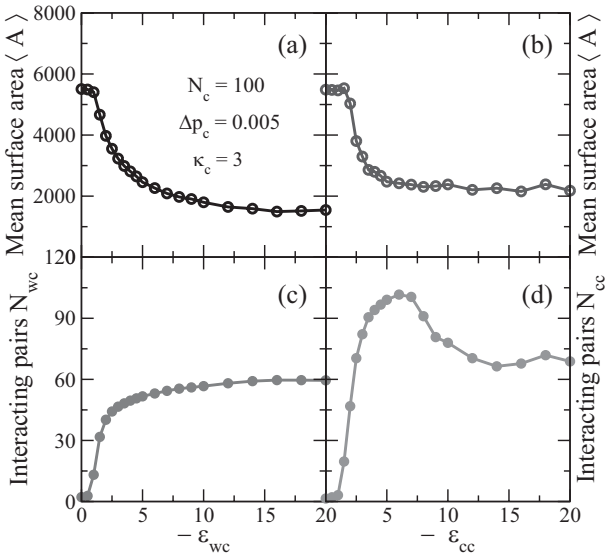

Figure 11. The mean surface area $\langle A \rangle$ and the number of interacting monomer pairs N_{xx} (where $x = w$ for a wall and $x = c$ for a cell) *versus* the energy parameter ε_{wc} or ε_{cc} for cells without EPS chains. Left column: One cell interacting with a wall; right column: two cells interacting with each other.

Interactions with EPS Chains

The presence of EPS chains will affect the way cells interact with each other and with a wall, as we shall see in this section. Of course, these interaction parameters must be chosen to favor the growth of cohesive colonies whose elements do not diffuse away from each other with time.

Cell–Wall–EPS Interactions

We first examine the case of a single cell attracted to a wall by a the short-range interaction energy ε_{wc} (see Figure 11a and c, as well as Figure 13a). The number of monomers interacting directly with the wall, N_{wc}, increases very quickly at first, but the rate of increase slows down considerably when $\varepsilon_{wc} < -2$. Moreover, the mean surface area of the cell, $\langle A \rangle$, decreases very rapidly passed this point. In other words, we have strong and nonphysical cell deformation below a certain critical value $\varepsilon_{wc}^* \simeq -2$.

We now examine the impact of EPS chains on the interaction of a single cell with a wall. In order to simplify the analysis, we study three possible situations: (i) $\varepsilon_{we} = 0$ and $\varepsilon_{wc} < 0$; (ii) $\varepsilon_{wc} = 0$ and $\varepsilon_{we} < 0$ varies; and finally (iii) $\varepsilon_{we} \leq \varepsilon_{wc} < 0$. The average cell surface area and the number of interacting monomer pairs are plotted in Figure 12, as a function of the relevant interaction

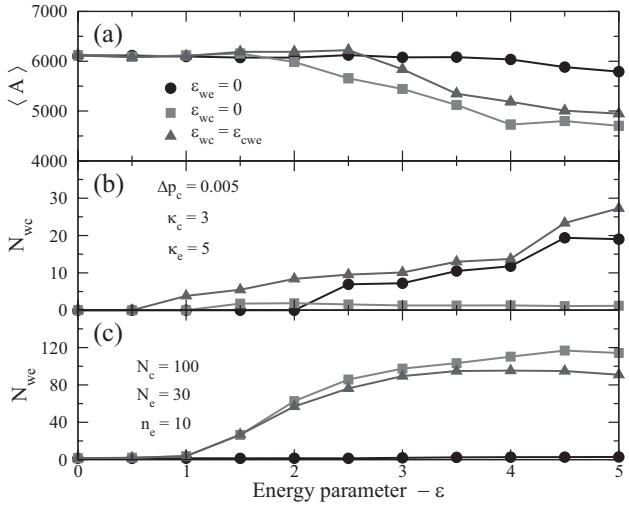

Figure 12. The mean cell surface area $\langle A \rangle$ and the number of interacting monomer pairs N_{xx} (where $x = $ w for a wall, $x = $ c for a cell and $x = $ e for an EPS monomer) *versus* the relevant attractive energy parameter (either ε_{wc} or ε_{we}) for cells with EPS chains (the simulation details are given in the figure).

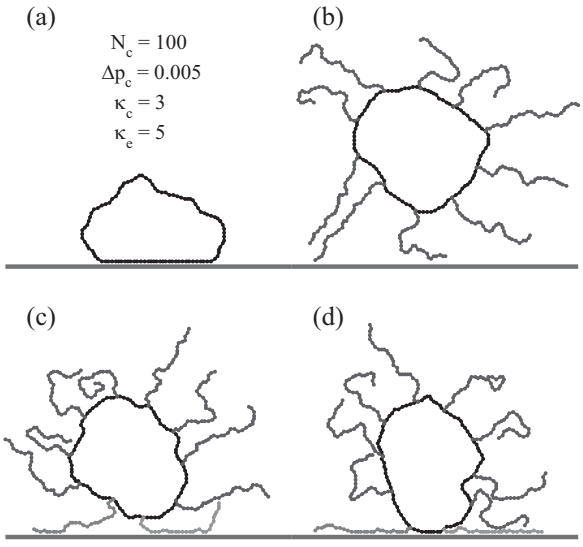

Figure 13. Schematic pictures of cells near a wall under different conditions. (a) A naked cell for a moderate attractive wall–cell interaction parameter $\varepsilon_{wc} = -2.0$. (b–d) Snapshots of cells with $n_e = 10$ EPS chains of size $N_e = 30$. The energy parameters are (b) $\varepsilon_{wc} = -2.0$ and $\varepsilon_{we} = 0.0$; (c) $\varepsilon_{wc} = 0.0$ and $\varepsilon_{we} = -1.5$, (d) $\varepsilon_{wc} = \varepsilon_{we} = -1.5$.

parameter for each of these cases, while Figure 13(b–d) illustrate some examples of cell shapes.

Case (i), where $\varepsilon_{we} = 0$, corresponds to a situation where the EPS brush represents an entropic barrier that limits the cell–wall interactions. As a result, the cells do not adsorb on the wall unless, i.e., $\varepsilon_{wc} \lesssim -2$, as illustrated in Figure 13(b). In fact, the cell shapes are not deformed even under strong cell–wall attraction. Case (ii), where we now have only EPS–wall interactions, corresponds to a case where the cells adsorb to the wall solely via their polymer brush (see Figure 13c). Again, we need a minimum interaction parameter ε_{we} before adsorption starts. When $\varepsilon_{we} < -2$, even the cell deforms in response to the strong EPS–wall interactions. We note that the food particles may diffuse between the cell membrane and the wall surface here; this will help the cells that are deep in the colony to grow. Finally, we look at case (iii) with $\varepsilon_{we} \leq \varepsilon_{wc}$; as shown in Figure 13(d), the cell membrane and the EPS chains then compete for access to the wall. Again, the mean surface area of the cell decreases when the interaction parameters exceed about -2.5. Therefore, we conclude that the magnitude of cell–wall–EPS interaction potential parameters must be kept under $\simeq -2.5$.

Cell–Cell–EPS Interactions

Let us now consider two interacting cells in the absence of EPS chains. Similar to the previous case of wall–cell interactions, the mean cell surface area decreases sharply when $\varepsilon_{cc} \leq -2.5$, as shown in Figure 11(b). The number of interacting pairs, N_{cc} reaches a maximum at $\varepsilon_{cc} \approx -5.0$ and decreases slightly beyond that point (Figure 11d). When the interaction is strong, the interface between the two cells tend to orient along the $\pm 45^\circ$ lattice directions in order to maximize the number of monomer–monomer contacts (see, e.g., Figure 14a). It is important to avoid these BFA artifacts.

Under weak cell–EPS attractive interactions (e.g., $\varepsilon_{ce} = -1.0$, as shown in Figure 14b) an EPS chain does not interact with the cell very often; however, strong cell–EPS attractions lead to EPS chains that are irreversibly bound to the cell surface, as shown in Figure 14(c). The latter effect induces unrealistic cell shapes and quenches all dynamics; it should be avoided. Obviously, both high EPS grafting densities and long chain lengths enhance this effect.

If two cells are close to each other, an EPS chain can bind simultaneously to both cells, thus keeping them together. This effect is crucial for the formation of colonies where the cells are embedded in an EPS matrix that acts are the glue that keep the colony together. However, if ε_{ce} is too strong (see, e.g., Figure 14d), the bridging interaction deforms the two cells and the latter can stay in a locked position for extremely long times. In other words, we need moderate EPS–cell interactions in order to model realistic biofilms.

Similar to what we did in the previous section for the cell–wall–EPS interactions, we will simplify the analysis of the cell–EPS–cell interactions by studying three situations of interest for biofilms: (i) $\varepsilon_{ce} = \varepsilon_{ee} = 0$ and $\varepsilon_{cc} < 0$; (ii) $\varepsilon_{cc} = \varepsilon_{ee} = 0$ and $\varepsilon_{ce} < 0$; and finally (iii) $\varepsilon_{ce} = \varepsilon_{cc} = 0$ and $\varepsilon_{ee} < 0$. The mean cell surface area and the number of

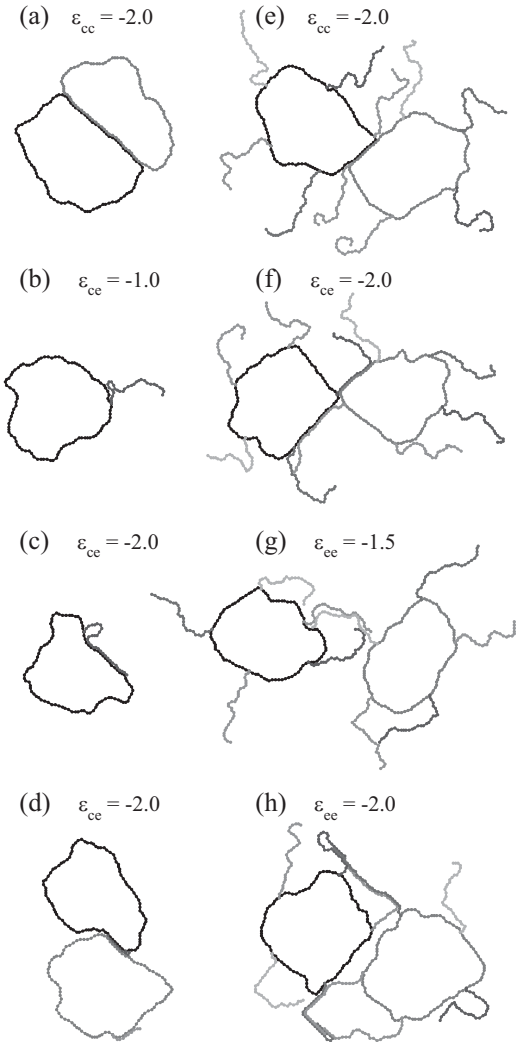

Figure 14. Schematic pictures of interacting cells and EPS polymer chains under various conditions. The relevant interaction parameters are ε_{cc}, ε_{ce}, and ε_{ee}. The values of the nonzero parameters are shown in the figure for each case. The other simulation parameters are as same as those used for Figure 13. (a) Two identical naked cells interact via a relatively strong attractive parameter $\varepsilon_{cc} = -2.0$. (b) and (c) A long EPS chain ($N_e = 30$) interacts with the cell to which it is attached. (d) Two cells with one short EPS chain each (size $N_e = 10$) are glued via the EPS chain sitting between them. (e–h) Two cells with $n_e = 5$ EPS chains (of size $N_e = 30$) each. Situation (g) is the best situation for the growth of a realistic biofilm. Note that in these four cases, the EPS chains were not allowed to interact with the cell to which they were attached.

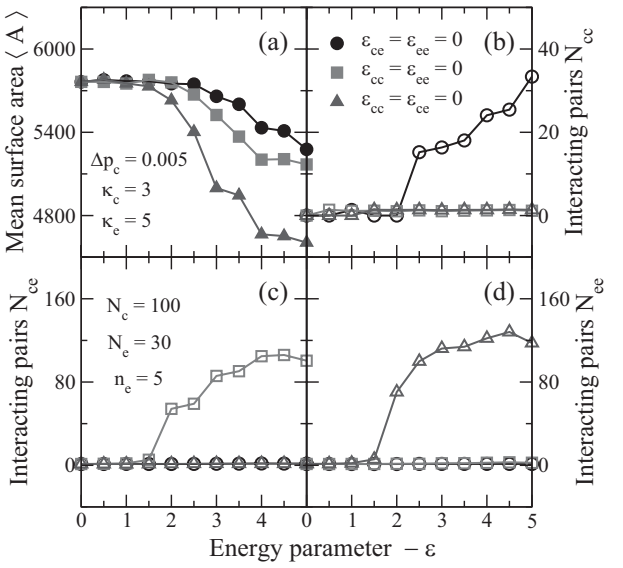

Figure 15. The mean cell surface area $\langle A \rangle$ and the number of interacting monomer pairs N_{xx} (where $x = c$ for a cell and $x = e$ for an EPS monomer) *versus* the relevant attractive energy parameter (either ε_{cc}, ε_{ee}, or ε_{ce}) for two interacting cells covered with EPS chains (the simulation details are given in the figure).

interacting monomer pairs are plotted in Figure 15, as a function of the relevant interaction parameter for each of these cases, while Figure 14(e–h) illustrate some cell shapes.

For case (i), i.e., when cell–EPS and EPS–EPS interactions are 0, increasing the cell–cell interaction parameter ε_{cc} leads to a situation similar to what we say previously for naked cells (see also the snapshot in Figure 14e), although the existence of the two opposing EPS brushes limits the cell–cell contact interface. This is similar to the entropic repulsion that exists between hairy colloidal particles. Since cells are rarely in direct contact in a biofilm, we will use a relatively small value of $\varepsilon_{cc} = -1$ in our simulations.

When only the cell–EPS attractions are included (i.e., $\varepsilon_{ce} < 0$, case (ii)), the EPS chains bridge between the cells and can get rather close, as shown in Figure 14(f). The situation would obviously be similar with free EPS chains. In order to allow the EPS-based gel to fully form between the cells, we will also use a rather small value of $\varepsilon_{ce} = -1$ for this parameter.

Finally (case (iii)), if only EPS–EPS interactions are taken into account, multiple EPS chains tend to interact and sometimes pile-up on each other (see Figure 14g and h), especially if $\varepsilon_{ee} \lesssim -2.0$.

Examples of EPS–Cell Biofilms

The values of the various interaction parameters must be carefully chosen in order to avoid undesirable effects during the growth of the biofilm colony. Unlike the examples discussed in the previous section, however, the situation inside a biofilm is characterized by multiple cells interacting with each other via a large number of EPS chains. Although useful, examples using only two cells cannot perfectly represent a situation where a cell is surrounded by other cells and cannot escape from the colony. Because of the anisotropy of the interaction between a pair of cells

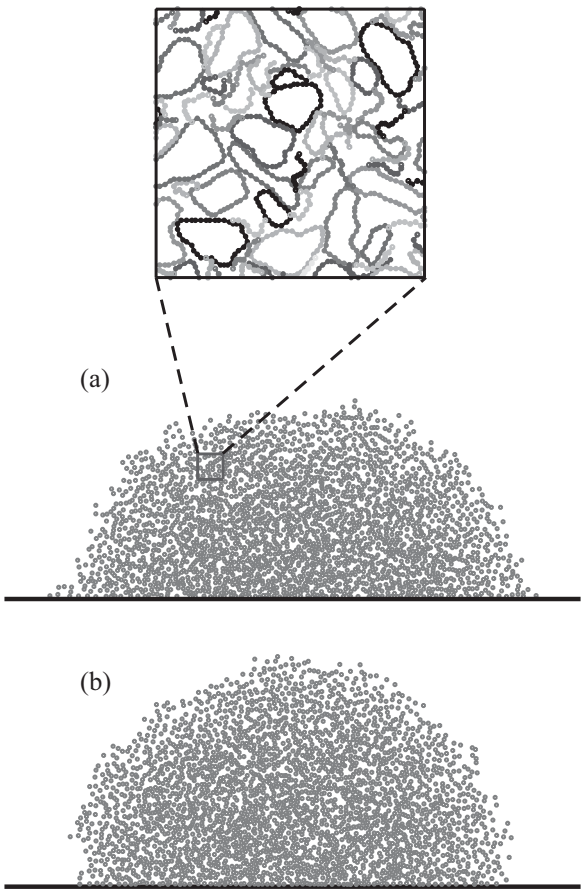

Figure 16. Two examples of biofilm colonies containing both cells and the polymeric EPS chains that they produced during their growth. For the sake of clarity, the nutrient particles and the EPS chains are not shown. Each cell is represented by an open circle. Inset: A zoom on a small 150×150 area showing the details. (a) The values of the parameters used for this simulation are listed in Table 1; (b) same parameters, except for $\varepsilon_{we} = 0.0$.

(hairy or not), one needs strong interactions in order to keep them in contact. In other words, weaker interactions between the cells and the EPS chains are sufficient (and preferable) when simulating the growth of a colony. However, it is crucial to have strong interactions with the wall in order to keep the colony attached to the surface, especially during the early stages. In practice, $\varepsilon_{wx,(x=c,e)} = -2.0$ and $\varepsilon_{xx,(x=c,e)} = -0.5$ or -1.0 appear to be reasonable choices.

Two typical biofilm colonies with moderate cell–cell, cell–EPS, and EPS–EPS attractive interactions are illustrated in Figure 16. The list of parameters is given in Table 1 (note that we allowed each cell to synthesize only one EPS chain before it divides). Reservoirs of food particles were located on each sides of the initial naked cell attached to the bottom wall; the reservoirs were both of width $L/10$, where $L = 6\,000$ is the width of the box (the upper wall, or ceiling, is at a distance 3 000 from the bottom one). The resulting

Table 1. A complete list of the parameters used to simulate the colonies shown in Figure 16(a).

N_c^0	N_e^{max}	κ_c	κ_e	Δp_c
20	10	3	5	0.005
ε_{wc}	ε_{we}	ε_{cc}	ε_{ce}	ε_{ee}
-2.0	-2.0	-1.0	-1.0	-1.0
N_{cs}^{max}	ρ	Γ_{cs}^0	Γ_c^0	Γ_e^0
20	0.04	1.0	0.02	0.5

colony, obtained after 6×10^6 MCS and shown in Figure 16(a), contains 2 509 cells of different ages and sizes, together with 5019 EPS chains. The inset shows how the EPS chains organize to form the matrix in which the cells are embedded. The spacing between the cells allows for diffusion of food into (and waste material out of) the core of the biofilm.

It is interesting to note that the nature of the wall-colony contact can change if the parameters are changed. In Figure 16(a), the strong EPS–wall interactions lead to a contact angle smaller of $\sim 50^\circ$, typical of a hydrophilic interaction; while Figure 16(b) shows the colony formed when we turn off this interaction. The contact angle is now $\gtrsim (\pi/2)$, signaling a qualitative change to a more hydrophobic-like situation.

Conclusion

Our LMC simulation model is based on a novel approach that treats cells as autonomous thermodynamic and mechanical agents. In the current study, we have extended our 2D biofilm model[34] to include EPS, a key ingredient of biofilms. In order to find the proper values for the structural parameters needed to model realistic cells and colonies, we investigated the physical characteristics of cells in the presence of EPS chains. These studies mainly looked at cell swelling and EPS stretching. Key factors, such as cell size, EPS chain length and density, osmotic pressure difference, cell membrane and EPS chain bending rigidity, were systematically studied. The cell membrane bending rigidity and osmotic pressure difference are the two most important parameters which control the structure of cells. However, the presence of EPS chains increases the complexity of the problem. The EPS-related parameters need to be carefully chosen to avoid any nonphysical or unrealistic cell properties and/or BFA artifacts. In our study, we found that the parameter values of $\kappa_c = 3.0$ and $\Delta p_c = 0.005$ provide excellent results when simulating round-shape cells, i.e, this choice produces realistic mechanical, biological, and thermodynamic properties for our autonomous cells.

The EPS chain bending rigidity plays a relatively minor role when we look at single cell properties, but it is likely to be a crucial element in the biofilm colony where cells are embedded in the self-assembled EPS matrix. The choice of the EPS bending rigidity parameter $\kappa_e = 5.0$ allowed us to obtain mechanical properties that one would expect for semi-flexible EPS molecules; this value also prevented the collapse of EPS chains in crowded environments. We also found that strong attractive interactions among the various elements of the model tend to lead to nonphysical effects, and must therefore be avoided. In order to make the model more realistic (so that it better represents real biofilms), none of the interaction energy parameters should exceed -2.0.

During the formation of a large biofilm colony, some cells may die for reasons that include (i) old age; (ii) starvation; or (iii) chemical/biological attacks. All of these effects, as well as waste generation, metabolism, hibernation, mutations, motility, and chemotaxis have now been added to our model. Our future work will thus focus on the growth of complex multi-species colonies in the presence of these more complex phenomena. Moreover, biofilms use quorum sensing[42] to coordinate certain behaviors; this type of signaling process is based on the local density of the bacterial population. Clearly, the colony morphology can be quite affected by such a collective process. We believe that our model provides an interesting and a novel way to look at the evolution of biofilms since it explicitly includes the thermodynamic and mechanical properties of the EPS molecules.

Acknowledgements: We would like to acknowledge fruitful discussions with J. Dutcher (University of Guelph). The authors would also like to acknowledge the contributions of Drs. Yergou B. Tatek, Anand S. Bhandar, and Lixin Zhan to previous versions of this model. We would also like to thank HPCVL, SharcNet, and SciNet for computing resources. This work was partially supported by the Advanced Food and Materials Network (AFMnet) as well as by a University of Ottawa research grant to Gary W. Slater.

Received: March 18, 2011; Revised: June 2, 2011; Published online: July 22, 2011; DOI: 10.1002/mats.201100030

Keywords: bacteria; biofilm; cell adhesion; extracellular polymeric substance; lattice Monte–Carlo simulation

[1] R. Kolter, R. Losik, *Science* **1998**, *280*, 226.
[2] D. G. Davies, M. R. Parsek, B. Iglewski, J. W. Costerton, E. P. Greenberg, *Science* **1998**, *280*, 295.
[3] Q. Wang, T. Zhang, *Solid State Commun.* **2010**, *150*, 1009.
[4] J. W. T. Wimpenny, R. Colasanti, *FEMS Microbiol. Ecol.* **1997**, *22*, 1.
[5] S. W. Hermanowicz, *Water Sci. Technol.* **1998**, *37*(4–5), 219.
[6] S. W. Hermanowicz, *Water Sci. Technol.* **1999**, *39*(7), 107.
[7] S. W. Hermanowicz, *Math. Biosci.* **2001**, *169*, 1.
[8] S. W. Hermanowicz, in *Biofilms in Wastewater Treatment: An Interdisciplinary Approach* (Eds: S. Wuertz, P. A. Wilderer, P. L. Bishop), International Water Association Publishing, **2002**, pp. 1–18.
[9] C. Picioreanu, M. C. M. van Loosdrecht, J. J. Heijnen, *Biotechnol. Bioeng.* **1998**, *57*, 718.
[10] C. Picioreanu, M. C. M. van Loosdrecht, J. J. Heijnen, *Biotechnol. Bioeng.* **1998**, *58*, 101.
[11] C. Picioreanu, M. C. M. van Loosdrecht, J. J. Heijnen, *Water Sci. Technol.* **1999**, *39*(7), 115.
[12] C. Picioreanu, M. C. M. van Loostrecht, J. J. Heijnen, in *Community Structure and Co-operation in Biofilms* (Eds: D. G. Allison, P. Gilbert, H. M. Lappin-Scott, M. Wilson), Cambridge University Press, Cambridge, UK **2000**, pp. 129–166.
[13] D. R. Noguera, G. Pizarro, D. A. Stahl, B. E. Rittmann, *Water Sci. Technol.* **1999**, *39*(7), 123.
[14] G. Pizarro, D. Griffeath, D. R. Noguera, *J. Environ. Eng.* **2001**, *127*, 782.
[15] S. M. Hunt, M. A. Hamilton, J. T. Sears, G. Harkin, J. Reno, *Microbiology* **2003**, *149*, 1155.
[16] S. M. Hunt, E. M. Werner, B. Huang, M. A. Hamilton, P. S. Stewart, *Appl. Environ. Microbiol.* **2004**, *70*, 7418.
[17] S. M. Hunt, M. A. Hamilton, P. S. Stewart, *Water Sci. Technol.* **2004**, *52*(7), 143.
[18] J.-U. Kreft, G. Booth, J. W. T. Wimpenny, *Microbiology* **1998**, *144*, 3275.
[19] J.-U. Kreft, C. Picioreanu, J. W. T. Wimpenny, M. C. M. van Loosdrecht, *Microbiology* **2001**, *147*, 2897.
[20] J.-U. Kreft, J. W. T. Wimpenny, *Water Sci. Technol.* **2001**, *43*(6), 135.
[21] C. Picioreanu, J.-U. Kreft, M. C. M. van Loosdrecht, *Appl. Environ. Microbiol.* **2004**, *70*, 3024.
[22] C. Picioreanu, J.-U. Kreft, M. Klausen, J. A. J. Haagensen, T. Tolker-Nielsen, S. Molin, *Water Sci. Technol.* **2005**, *55*(8–9), 337.
[23] J. B. Xavier, C. Picioreanu, M. C. M. van Loosdrecht, *Environ. Microbiol.* **2005**, *7*, 1085.
[24] J. B. Xavier, C. Picioreanu, M. C. M. van Loosdrecht, *Biotechnol. Bioeng.* **2005**, *91*, 651.
[25] J. B. Xavier, M. K. de Kreuk, C. Picioreanu, M. C. M. van Loosdrecht, *Environ. Sci. Technol.* **2007**, *41*, 6410.
[26] O. Wanner, W. Guger, *Biotechnol. Bioeng.* **1986**, *28*, 314.
[27] B. D. Wood, S. Whitaker, *Biotechnol. Bioeng.* **2000**, *64*, 656.
[28] J. Dockery, I. Klapper, *SIAM J. Appl. Math.* **2002**, *62*, 853.
[29] H. J. Eberl, C. Picioreanu, J. J. Heijnen, M. C. M. van Loosdrecht, *Chem. Eng. Sci.* **2000**, *55*, 6209.
[30] H. J. Eberl, D. F. Parker, M. C. M. van Loosdrecht, *J. Theor. Med.* **2001**, *3*, 161.
[31] E. Alpkvist, N. C. Overgaard, S. Gustafsson, A. Heyden, *Water Sci. Technol.* **2004**, *49*(11–12), 187.
[32] E. Alpkvist, C. Picioreanu, M. C. M. van Loosdrecht, A. Heyden, *Biotechnol. Bioeng.* **2006**, *94*, 961.
[33] E. Alpkvist, I. Klapper, *Bull. Math. Biol.* **2007**, *69*, 765.
[34] Y. B. Tatek, G. W. Slater, *Phys. A* **2006**, *362*, 382.
[35] J. Wingender, R. C. Flemming, T. R. Neu, in *Microbial Extracellular Polymeric Substances* (Eds: J. Wingender, T. R. Neu, R. C. Flemming), Springer, Berlin **1999**, pp. 1–19.

[36] R. C. Flemming, J. Wingender, in *Encyclopedia of Environmental Microbiology*, Vol. 3 (Ed: G. Bitton), Wiley, New York **2002**, pp. 1223–1231.
[37] I. Carmesin, K. Kremer, *Macromolecules* **1988**, *21*, 2819.
[38] N. Metropolis, A. W. Rosenbluth, M. N. Rosenbluth, A. H. Teller, E. Teller, *J. Chem. Phys.* **1953**, *21*, 1087.
[39] M. Breidenich, R. R. Netz, R. Lipowsky, *Europhys. Lett.* **2000**, *49*, 431.
[40] T. Bickel, C. Marques, *Phys. Rev. A* **2000**, *62*, 1124.
[41] M. Laradji, *J. Chem. Phys.* **2004**, *121*, 1591.
[42] M. R. Frederick, C. Kuttler, B. A. Hense, H. J. Eberl, *Theor. Biol. Med. Model.* **2011**, *8*, 8.